

European tree-ring isotopes indicate unusual recent hydroclimate

Mandy B. Freund ^{1,2,3,4,5}✉, Gerhard Helle ⁴, Daniel F. Balting ^{4,6}, Natasha Ballis ^{3,7},
Gerhard H. Schleser⁸ & Ulrich Cubasch⁵

In recent decades, Europe has experienced more frequent flood and drought events. However, little is known about the long-term, spatiotemporal hydroclimatic changes across Europe. Here we present a climate field reconstruction spanning the entire European continent based on tree-ring stable isotopes. A pronounced seasonal consistency in climate response across Europe leads to a unique, well-verified spatial field reconstruction of European summer hydroclimate back to AD 1600. We find three distinct phases of European hydroclimate variability as possible fingerprints of solar activity (coinciding with the Maunder Minimum and the end of the Little Ice Age) and pronounced decadal variability superimposed by a long-term drying trend from the mid-20th century. We show that the recent European summer drought (2015–2018) is highly unusual in a multi-century context and unprecedented for large parts of central and western Europe. The reconstruction provides further evidence of European summer droughts potentially being influenced by anthropogenic warming and draws attention to regional differences.

¹CSIRO Oceans and Atmosphere, Melbourne, VIC, Australia. ²School of Geography, Earth and Atmospheric Sciences, University of Melbourne, Parkville, VIC 3010, Australia. ³Climate and Energy College, University of Melbourne, Parkville, VIC 3010, Australia. ⁴German Research Centre for Geosciences, Climate Dynamics and Landscape Evolution, Potsdam 14473, Germany. ⁵Department of Earth Science, Institute for Meteorology, Freie Universität Berlin, 12165 Berlin, Germany. ⁶Alfred-Wegener-Institute, Bremerhaven 27570, Germany. ⁷Environmental Hydrology and Water Resources, Department of Infrastructure Engineering, University of Melbourne, Parkville, VIC 3010, Australia. ⁸Institute of Bio- and Geosciences IBG-3, Forschungszentrum Jülich, Jülich 52428, Germany. ✉email: mandy.freund@csiro.au

Europe is projected to experience direct and indirect impacts of continuing anthropogenic warming, particularly related to the hydrological cycle, such as droughts and floods^{1,2}. Severe drought conditions in the summers of 2003³, 2010, 2015⁴ and 2018 demonstrated the damaging and expensive impacts of widespread European droughts⁵. Flooding caused by extreme precipitation in 2021 showed the harmful nature and devastating impacts of hydroclimatic extremes on society. With anthropogenic warming projected to exacerbate the occurrence of hydrological extremes around the world^{6,7}, Europe faces large uncertainties in risks to its population, ecosystems and economies^{8,9}. Europe's vulnerability to hydroclimate extremes is further confounded by the complex interplay of spatially opposing trends¹⁰, a large degree of internal variability¹¹ and brevity of long-term spatiotemporal records.

The most recent European summer drought (2015–2019) has sparked a debate as to whether it is within the range of natural variability¹² or related to anthropogenic warming¹³. Long-term observations suggest that there had not been two consecutive summer droughts in central Europe in 250 years until 2018–2019¹⁴. Based on traditional tree-ring records and reanalysis products, the recent drought is well within the range of natural variability thus not unprecedented¹². By contrast, a long tree-ring isotope record from the Czech Republic indicates that the recent consecutive drought was unprecedented in the last two millennia¹³. It remains unclear whether this recent drought is part of natural climate variability or potentially a consequence of anthropogenic climate change. Obtaining a precise picture of the natural variability of the European hydroclimate is a challenge due to the sparse spatial coverage of moisture-sensitive proxy data¹⁵.

To understand the spatial complexity of the large-scale European hydroclimate, spatially explicit, long-term data sets are needed. Multi-century climate data are essential for the validation of climate models including comparisons to other paleoclimate, historical, and archaeological data sets. Tree-ring widths and maximum latewood density provide the longest and most replicated high-resolution records used in previous reconstructions of Holocene past climate¹⁵. However, tree-ring widths require statistical detrending, making it difficult to use them to reconstruct some aspects of low-frequency climate variability¹⁶. Furthermore, tree-ring width chronologies from European lowlands can display weak and ambiguous climate signals. In contrast, tree-ring stable isotopes are considered to be a more powerful proxy as they potentially require less statistical data treatment, and often exhibit clearer climate signals particularly in the temperate European lowlands^{13,17,18}.

In this study, we reconstruct European hydroclimate based on a network of tree-ring stable isotopes of oxygen and carbon ratios. The network combines up to 400-year long, annually resolved records of deciduous oaks from European lowlands and conifers from boreal and mountainous sites. This is the first time that stable isotope records from tree rings, with their so far untapped high climate reconstruction potential, are used to obtain a gridded spatial reconstruction of the European summer hydroclimate.

Results

European tree-ring isotope network. The tree-ring isotope network is composed of 26 individual, well-distributed sites from across Europe (Fig. 1a). Each location has a stable isotope record of carbon ($\delta^{13}\text{C}$) and oxygen ($\delta^{18}\text{O}$) derived from tree-ring cellulose obtained from old living trees using standard procedures of dendrochronological dating and cross-dating¹⁶ and stable isotope analyses¹⁹ (Methods). The network is composed of eight deciduous broadleaf oak stands (*Quercus spp.*) and 18 coniferous

stands (*Pinus*, *Juniperus*, *Larix*, *Cedrus*) ranging from elevations of 10–2200 m (Supplementary Table 1). Most of the broadleaf stands are concentrated in central-western Europe while the coniferous stands are mainly located at high latitudes and high elevations. The common period of all carbon and oxygen isotope records is 1850–1998 (Fig. 1b). Mass spectrometry of stable isotope ratios was conducted using pooled alpha-cellulose samples from at least four trees per site¹⁹. Coniferous species were measured using whole tree-ring wood material, whereas cellulose extraction for most oak sites was achieved on latewood only²⁰. Previous studies based on the isotope network^{20,21} and on single sites have revealed common climate signals across Europe^{22–29}, enabling a pooling of isotopic records derived from broadleaf trees and conifers into a single dataset.

Seasonal climate signal of the tree-ring isotope network.

Monthly correlation analysis with climate variables reveals a highly seasonal dependency of isotope records with summer conditions (JJA). While most $\delta^{18}\text{O}$ records are positively correlated with summer temperature and anti-correlated with precipitation, $\delta^{13}\text{C}$ records show the reverse climate response (Supplementary Figs. 1 and 2). Since both climate parameters are physically related and lower precipitation is mostly accompanied by high temperatures, it is difficult to separate out a specific forcing signal³⁰. This strong covariability of temperature and precipitation suggests that drought variability is a more appropriate climate parameter to exploit the combined $\delta^{18}\text{O}$ and $\delta^{13}\text{C}$ climate information.

The majority of isotope sites across Europe display the highest seasonal correlations with the Standardised Precipitation-Evapotranspiration Index³¹ (SPEI) in summer (Fig. 1c, d). Independent of latitude, elevation or species, all $\delta^{18}\text{O}$ records are most correlated with SPEI in summer (Fig. 1c). The only exception is the Turkish site (Isibeli), which shows the highest correlation with spring conditions²³. Carbon records (Fig. 1d) exhibit similar seasonal correlations with predominantly summer SPEI except for three sites (Vinuesa, Niepolomice and Col Du Zad). Across all sites, one or both isotopic records represent summer conditions during the current year of ring formation as a key influence on tree-ring isotope variability. Comparing the climate signals from isotopes with tree-ring widths shows substantial differences (Fig. 1e). Classical European tree-ring records³² mirror temperature and precipitation extremes but show diverse seasonal responses, with a greater influence of the cold season corresponding to greater continentality³³. Even though a large proportion of European tree-ring width chronologies include a summer SPEI signal, there are spatial biases towards high-elevation sites such as the Alps or Pyrenees or climatically extreme sites in the far north or south. Lagged and carry-over effects that are present in many traditional tree-ring width chronologies limit the ability to retrieve a coherent continent-wide seasonal drought signal for Europe. The tree-ring isotope records promise a more homogeneous seasonal drought signal across the wide ranges of altitudes and latitudes and a better representation of low- to high-frequency variability (Supplementary Fig. 7), making them superior proxies for spatial reconstructions of hydroclimate variability compared to traditional tree-ring parameters¹⁵.

European hydroclimate reconstruction. We employ the well-established and tested point-by-point regression approach³⁴ to spatially reconstruct summer hydroclimate variability (July–August SPEI) for the past 400 years. Similar to the climate field reconstruction efforts using tree-ring widths and maximum latewood density in Europe¹⁵ and other regions^{34,35}, a nested and

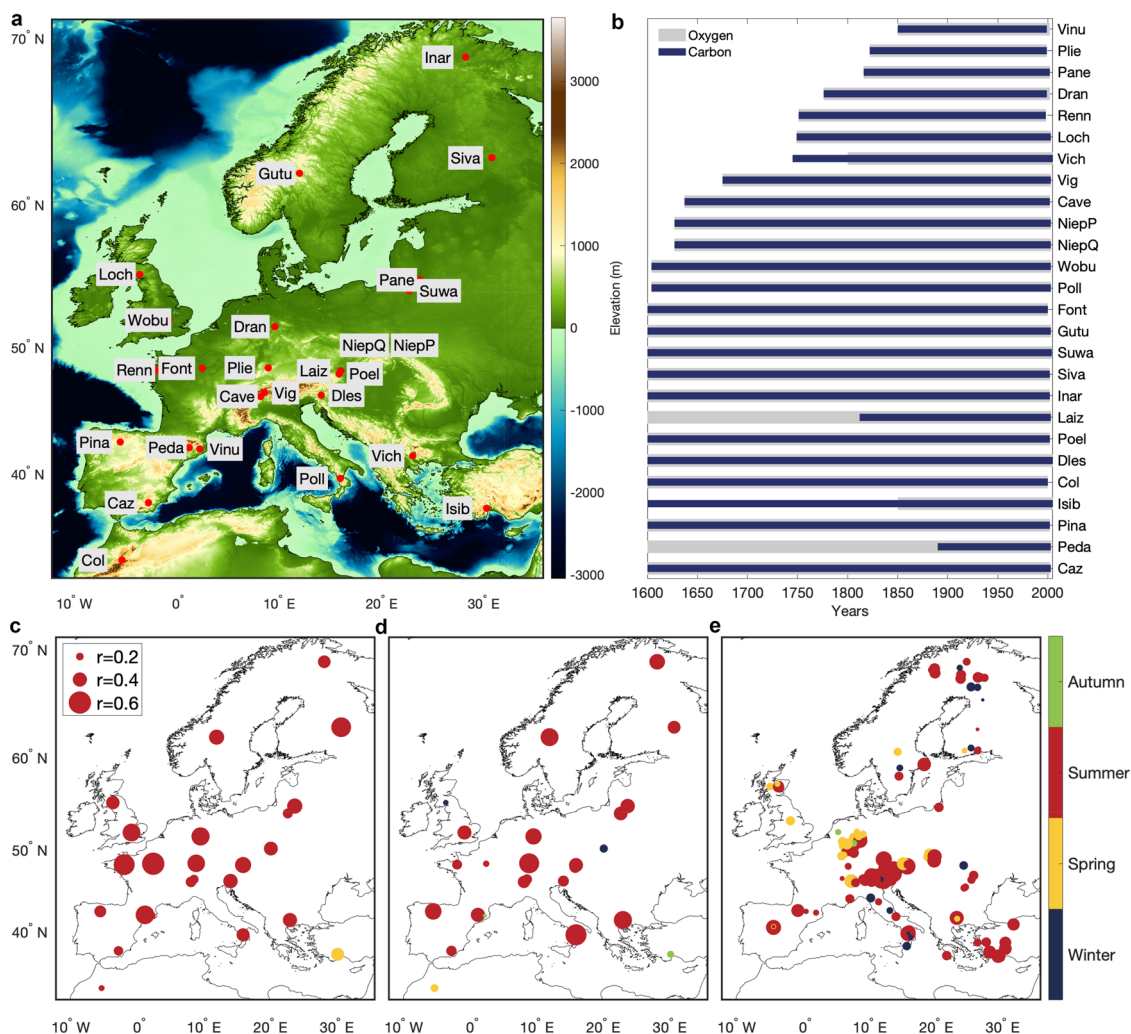


Fig. 1 Overview of the European tree-ring isotope network. **a** Spatial distribution of the tree sites across Europe with annually resolved isotope records of $\delta^{18}\text{O}$ and $\delta^{13}\text{C}$. **b** Temporal distribution of $\delta^{18}\text{O}$ and $\delta^{13}\text{C}$ records as bars. **c–e** Seasonal response of carbon, oxygen and tree-ring records⁶², respectively, with SPEI-2. Shown is the highest leading seasonal correlation with SPEI. Over the 1901–1998 period the highest correlation for each site is assigned to the closest gridboxes within 60 km.

correlation-weighted regression approach is applied to split calibration (1914–1963) and verification (1964–1998) periods (Methods). The reconstruction explains up to 64% of summer SPEI variability in western-central Europe and approximately 30% averaged across the continent (Fig. 2a). Validation statistics demonstrate excellent agreement between instrumental and reconstructed SPEI at interannual and decadal timescales, with the strongest agreement in western, northern and parts of southern Europe (Fig. 2b). Most of the calibration and verification statistics indicate a significant and temporally stable climate-isotope relationship. The positive values of the reduction of error (RE) and the coefficient of efficiency (CE) at over 85% and 75% of all gridpoints (Fig. 2c, d), respectively, further highlight the robustness of the reconstructions. The skill of the reconstruction is strikingly good in parts of western and northern Europe, the skill is less in high-elevation regions such as the Carpathian Mountains, the Scandinavian Mountains and the Scottish Highlands, and in low-elevation regions such as north-east Germany and parts of Poland, potentially due to the lack of local tree-ring isotope sites, the regions being continental fringe locations, inconsistent climate-isotope relationships, or heterogeneous climate data (Supplementary Fig. 4). Long historical records and paleoclimate reconstructions^{13,15,36,37} further corroborate the

SPEI reconstruction for the pre-instrumental period. There is high covariance between historical temperature records and the SPEI reconstruction on continental and regional scales, and high covariance between historical precipitation records and the SPEI reconstruction on local scales (Supplementary Table 2). Spatially resolved reconstructions of precipitation, PDSI and temperature are also highly correlated with our SPEI reconstruction (Supplementary Fig. 4). This provides additional assurance that our European summer SPEI reconstruction captures a large proportion of temperature and precipitation variability, is well verified during instrumental and pre-instrumental periods and is in parts, superior to existing reconstruction efforts.

European droughts and change points. The continental SPEI reconstruction shows variability on different timescales ranging from interannual to multi-decadal (Fig. 3a). Mostly wet conditions prevailed in the early seventeenth century exemplified by the first year of the reconstruction (1600), followed by generally drier conditions for almost two centuries. These generally drier conditions prevailed until the mid-nineteenth century, alternating with extreme wet conditions on an interdecadal scale. During this period, wet anomalies lasting several years, such as around 1840 or 1870, were rare. This is in contrast to the twentieth century,

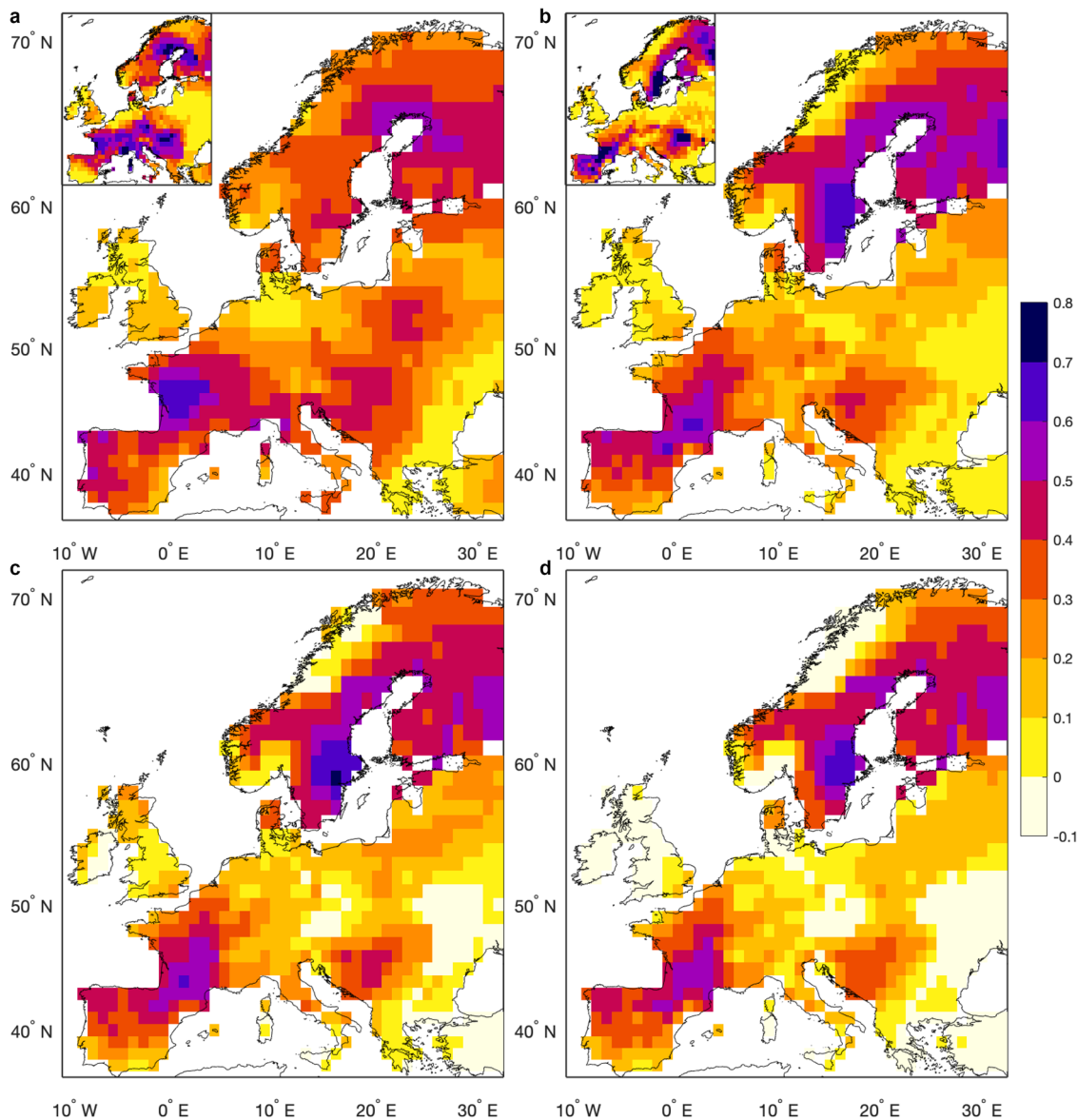


Fig. 2 Spatial reconstruction statistics. Calibration and verification statistics for the SPEI reconstruction. Explained variance (R^2) of **a** the calibration period (median CRSQ = 0.31) and **b** the verification period (median VRSQ = 0.22) on interannual and decadal timescales (insets) using a 5-year moving average filter. **c** Reduction of error of the calibration period (median RE = 0.20). **d** Coefficient of efficiency of the verification period (median CE = 0.15).

during which wet and dry phases commonly spanned 5 or more years, such as in the 1950s and 1960s, and there appeared to be greater decadal variability. The reconstruction reveals the spatial signature of well-known extreme years. For example, the significantly cold, wet summer of 1816, often referred to as ‘the year without summer’³⁸, which corresponded with the Tambora eruption in Indonesia thought to have cooled the world by 2–3 °C³⁹. The SPEI reconstruction (Fig. 3a, inset) reveals very wet conditions in western Europe during this particular year, yet those parts of western Europe (Spain) and northern Europe were not affected. Other large volcanic eruptions such as the Laki eruption (1773–1784) and the Krakatoa eruption (1883) show no coherent impact on the summer SPEI (Supplementary Fig. 5).

Change point analysis of the continental SPEI reconstruction reveals three distinct phases (Fig. 3b). The first phase, from 1600 to 1652, is characterised by generally a wetter climate, with anomalously wet conditions spanning multiple years. These pluvial years are most apparent in western-central and northwest Europe (Fig. 3c). Shortly after the start of the

Maunder Minimum (1652), summer SPEI conditions shift to drier conditions, lasting over two centuries. This second phase is characterised by intense negative SPEI anomalies and a number of multi-year droughts. The Mediterranean, eastern and northern Europe are most affected by this change to drier summer conditions (Fig. 3c). By the end of the Little Ice Age, the third long-term change occurs and the third phase starts. Around 1875, after decades of generally drier conditions, the reconstructed SPEI changes significantly. Large parts of central and western Europe and the Mediterranean show milder summer conditions (Fig. 3c). These milder conditions prevail during the first half of the twentieth century until approximately the 1950s. In the second half of the twentieth century, we see a declining trend towards drier conditions, possibly linked to increasing temperatures, exemplified by the driest years on record (2003 and 2006) at the continental scale. These three distinct phases can, in part, also be found in other European reconstructions (Supplementary Fig. 6), but appear to be drought-specific features.

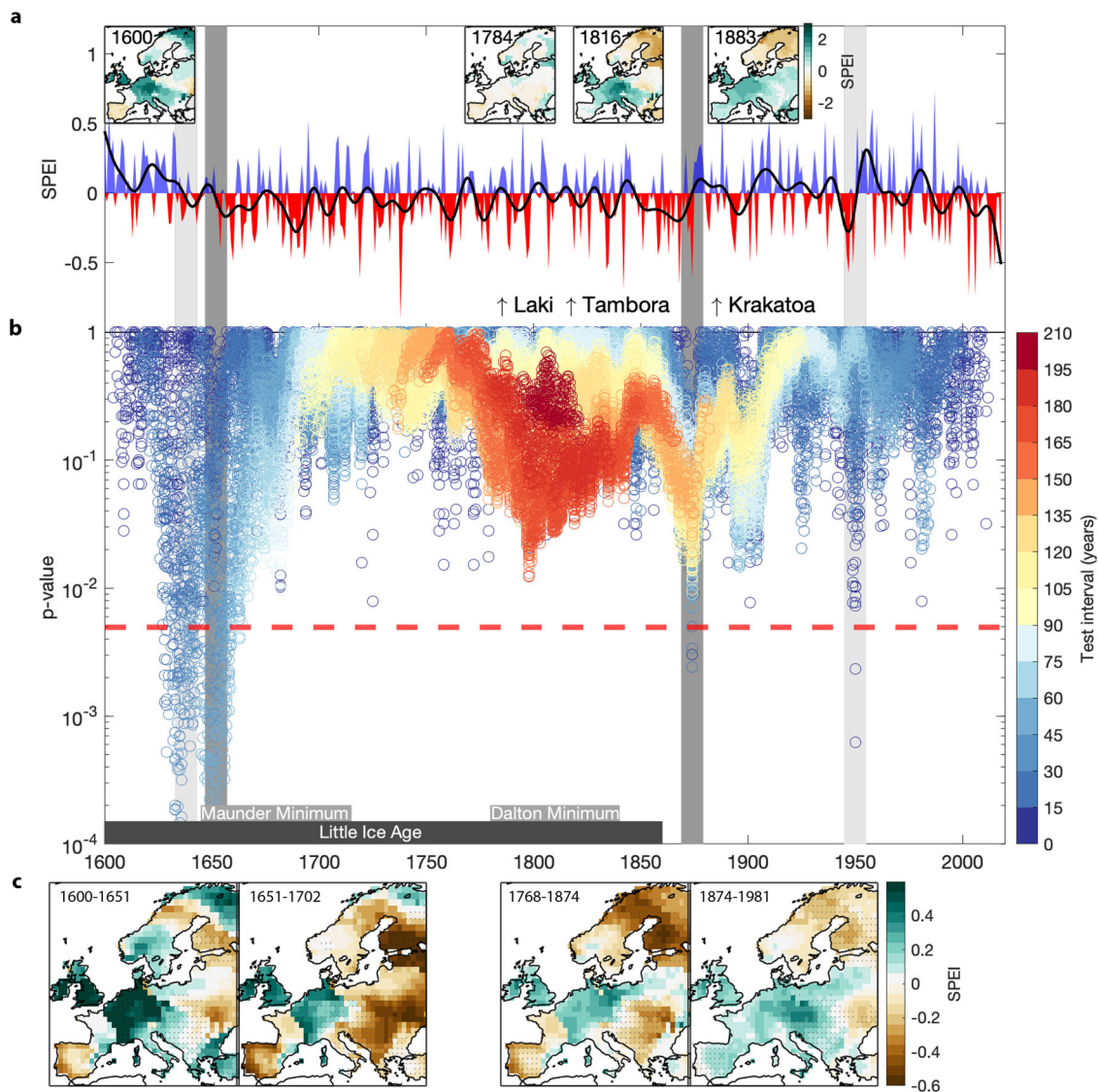


Fig. 3 Reconstructed European summer variability. **a** European field average of reconstructed SPEI (JA) from 1600 to 2018. A smoothed 13-year Chebyshev low-pass filter is shown as a black line. Insets show the spatial reconstructed SPEI for 1600, 1784, 1816 and 1883. **b** Change point analysis of European field average using the Wilcoxon rank-sum tests for sliding time intervals between 5- and 200-year time windows. The colour of a point corresponds to the tested time interval, and the year corresponds to the centre of the tested data. Significant change points are below the red horizontal line ($p < 0.01$). The Little Ice Age (≈ 1300 –1860 CE) and the Maunder Minimum (1645–1715) periods are highlighted. Vertical lines indicate significant long-term (dark, >30 years) and short-term (light) change points. **c** Average conditions before and after significant long-term change points in 1651 (left) and 1874 (right).

Recent trends and droughts. We use our SPEI reconstruction to place recently observed trends and droughts in the context of the past four centuries. Histograms summarise all 30- and 100-year linear trends in the European reconstruction (averaged across all gridpoints) from 1600 to 2018 (Fig. 4a, b). In the distributions of trends, we distinguish between pre-1970/1900 variability (grey), trends since 1970/1900 (light coloured) and the trend of the most recent 30 or 100 years (dark coloured) (Fig. 4a), recent trends vary in sign, highlighting a large degree of variability. The most recent trend is a slight tendency towards drier conditions; however, it is indistinguishable from the distribution of historical trends derived from the entire reconstruction. At the continental scale, there is no significant 30-year drying trend. In contrast, considering a 100-year window, there is a clear tendency towards drier conditions (Fig. 4b). Trends starting after 1900, including the most recent trend ending in 2018, are in the lower quartile range. These overall trends towards

drier conditions appear to be unusual, yet not unprecedented, considering the long-term context of the reconstruction. The spatial distributions of the recent trends (Fig. 4c, d) reveal that significant declines in the summer SPEI are mainly observed in southern Europe. In the latest 30-year period, parts of Spain and Italy experienced a significant decline in summer SPEI (Fig. 4c). When considering the trend over 100 years, this tendency towards drier conditions intensifies and expands to include large parts of southern, western and central Europe (Fig. 4d), including Spain, France, parts of Germany, Poland and Sweden. Fennoscandia is the only region that experienced a significant wetting trend in the past 100 years. This significant centennial wetting trend within the Arctic Circle contrasts sharply with the drying trends over the southern continental mainland. The spatial European drought reconstruction provides not only evidence of regional long-term trends but also helps to contextualise multi-year drought events such as the recent dry spells since 2015. Most

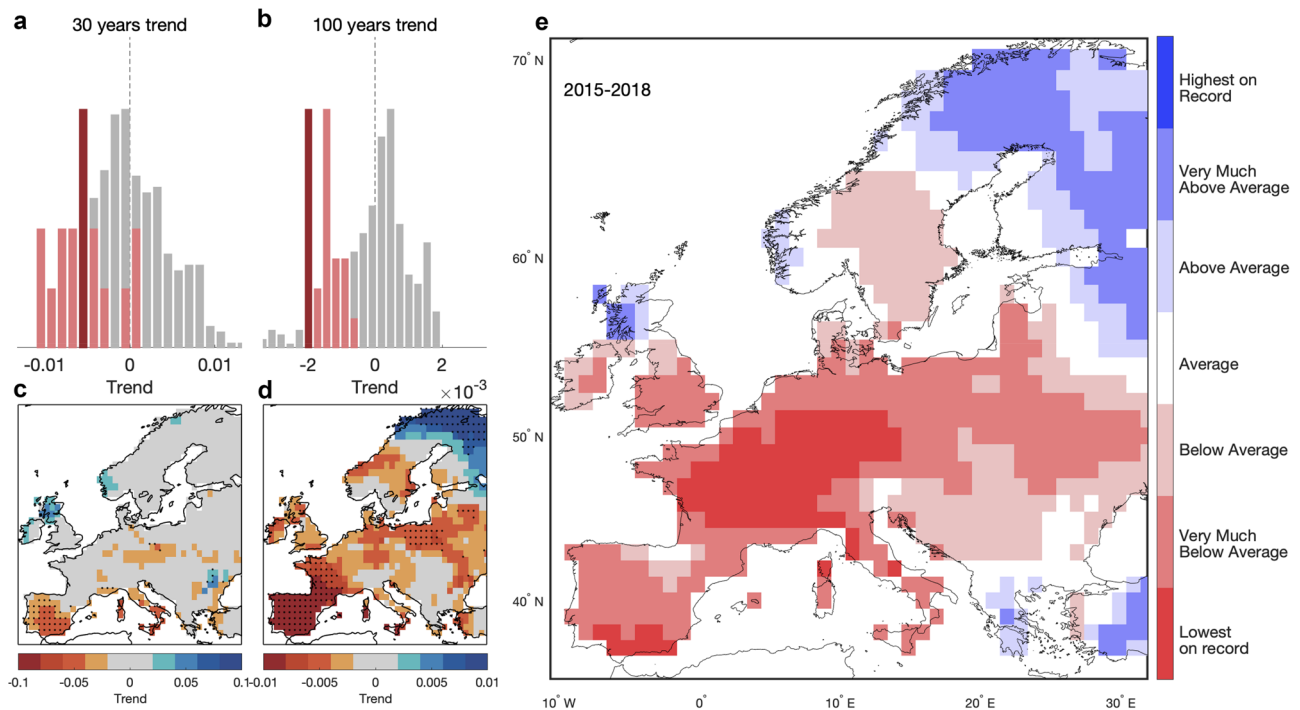


Fig. 4 Recent trends and drought. **a, b** Contextualising recent 30- and 100-year trends of average European SPEI (JA). Histograms show the full range of the trends (grey shaded bars) prior to 1970 for 30-year periods (**a**) and 1900 for 100-year periods (**b**). Recent periods are shown in light red, except the most recent period, which is shown in dark red. Bar heights are normalised by the maximum occurrence. **c, d** Recent trends of gridded SPEI of the most recent 30-year period (**c**) and 100-year period (**d**) ending in 2018. Stippling indicates statistically significant trends ($p < 0.05$). **e** The recent drought period (2015–2018) is shown as deciles considering the full period (1600–2018).

of the European mainland experienced unprecedented drought conditions between 2015 and 2018 with moisture conditions very much below average and in some places the lowest on record (Fig. 4e). Large parts of central and western Europe, southern Spain and parts of Italy encountered this recent 4-year drought episode, unprecedented relative to both the instrumental record and the past four centuries. In contrast, during this period, parts of northern Europe including Scotland and parts of Fennoscandia, as well as southeastern regions, including Greece and Turkey experienced unusually wet conditions. These opposing conditions highlight the importance of spatial climate reconstructions.

Our spatial reconstruction of summer drought conditions over Europe based on tree-ring isotope records provides evidence of historical changes and provides a unique long-term context for recent trends and drought events. We find that the most recent sequence of summer drought (2015–2018) is unprecedented in the past four centuries for large parts of Europe and is superimposed by long-term trends. This result corroborated and spatially extends the finding of the recently published Czech Republic summer reconstruction¹³. Our reconstruction also provides additional evidence of longer and possibly more severe droughts¹². We find that during the Maunder Minimum and at the end of the Little Ice Age⁴⁰, summer conditions across Europe were drier and multi-year drought episodes occurred frequently. This may have been due to the low solar activity at the time⁴¹, possibly similar to severe droughts during the Little Ice Age such as observed in the United States⁴². The observed tendency towards greater decadal SPEI variability and frequent multi-year pluvials following the end of the Little Ice Age⁴³ could be related to the sudden reversal in Holocene temperature records^{44,45}. To further confirm links between European drought conditions, solar forcing and anthropogenic warming, climate model simulations are currently being carried out within the CMIP6 framework, but the evaluation has not yet been finalised. At present, shortcomings

of climate models to adequately represent hydroclimatic conditions hinder a direct comparison^{7,12,13,46–50}. Our reconstruction is therefore providing a unique baseline for constraining past and recent changes and improving our understanding of droughts in a warming world.

Methods

Instrumental climate data. We use the Standardised Precipitation–Evapotranspiration Index (SPEI) as the instrumental target for our reconstruction. The SPEI is a multiscalar and multitemporal drought index which can quantify drought events on different timescales³¹. The global SPEI database⁵¹ ‘SPEIbase v2.6’ is calculated over the 1901–2018 period using precipitation and potential evapotranspiration data from the CRU TS4.03 dataset⁵². The potential evapotranspiration data is calculated based on CRU TS4.03 temperature, vapour pressure, cloud cover and wind field data, via the Penman–Monteith equation. On a spatial resolution of $1^\circ \times 1^\circ$, the SPEI combines the influence of precipitation and potential evapotranspiration to determine the accumulation of water deficit/surplus at different timescales ranging from short- (monthly) to medium-term moisture conditions and up to long-term (multi-annual) precipitation variability³¹.

Isotopic tree-ring records. We compiled a network of 26 individual tree sites of stable oxygen isotope ($\delta^{18}\text{O}$) ratios and carbon isotope ($\delta^{13}\text{C}$) ratios extracted from the corresponding tree-ring cellulose material. While the oxygen isotope records do not require any pre-processing, the carbon isotope records need to be adjusted to account for anthropogenic CO_2 emissions of strongly depleted $\delta^{13}\text{C}$ values. The use of the photosynthetic discrimination $\Delta^{13}\text{C}$ takes into account the decreasing $\delta^{13}\text{C}$ trend due to anthropogenic CO_2 emissions. It removes this offset and eliminates this imposed anthropogenic trend. In contrast to the physiological age-related trend, which influences tree-ring widths, the $\delta^{13}\text{C}$ records are influenced by the increasing anthropogenic trend of CO_2 in the atmosphere⁵³. Since industrialisation, the atmospheric CO_2 concentration has increased from approximately 280 ppm to almost 415 ppm, a rise of almost 50%. The burning of fossil fuels releases CO_2 originating from organic matter. This CO_2 is therefore depleted in ^{13}C resulting in a decline in the $^{13}\text{C}/^{12}\text{C}$ ratio of atmospheric CO_2 ⁵⁴. Accordingly, an atmospheric correction was applied to the tree-ring carbon based on ref.⁵⁵. The resulting records contain a small number of missing values (<1%), which we impute by the regularised expectation maximisation (RegEM) method⁵⁶. All the records were normalised to have zero mean and unit standard deviation.

SPEI reconstruction. We employ a nested principle component regression approach that fits principal component regression models to each set (nest) of tree-ring isotope records and the time series of the gridded SPEI dataset (JA SPEI-02). The Point-by-Point Regression method (PPR)⁵⁷ has previously been applied to traditional tree-ring networks including in Europe^{15,58}. Using the same well-tested regression reconstruction method allows for direct comparison.

Prior to regression analysis, the PPR method accounts for serial autocorrelation so that the predictand and the predictors are prewhitened prior to calibration. The modelled autocorrelation removed during calibration is added back to the reconstruction to preserve the temporal structure of the instrumental climate data. Single principle component regression models are then fitted for each of the 813 gridpoints and each nest of available proxy records. The pool of available proxy records is restricted to proxy sites within an 800-km radius from the target grid cell and are differentially weighted by the power of 0.5 of its correlation with the predictand variable. Final rescaling of lost variance during calibration relative to the original mean and standard deviation of the climate data is added back to the estimate and ultimately allows a seamless extension with recent climate data until 2018.

Change point and trend analysis. We perform change point analyses to identify periods of significant change using the Wilcoxon rank-sum test. The rank-sum test has been tested suitably for windowing approaches in climate data^{59,60}. Moving window tests of 5 years up to multi-decadal sampling duration are applied to the area-weighted drought reconstruction. To identify changes, tests for the difference in medians are determined by the significance of p values. Due to a large number of test realisations, the 95% confidence level is adjusted for the false discovery rate⁶¹. Linear trends were determined by the slope of a linear regression. The significance of trends in the reconstruction was assessed at the $p < 0.05$ confidence level using a one-sided Student's t -test, while accounting for lag-1 autocorrelation.

Data availability

Primary input and output data are archived by the National Oceanic and Atmospheric Administration (NOAA) for routine access and use. ISONET oxygen isotope data can be accessed at GFZ Data Services: <https://doi.org/10.5880/GFZ.4.3.2023.001> (18O) and <https://doi.org/10.5880/GFZ.4.3.2023.002> (13C). The reconstruction, statistics and additional information are available at: <https://doi.org/10.26188/21988628.v1>.

Code availability

The code associated with this paper is available on request from M.B.F.

Received: 13 January 2022; Accepted: 25 November 2022;

Published online: 08 February 2023

References

- Dai, A. Increasing drought under global warming in observations and models. *Nat. Clim. Change* **3**, 52–58 (2013).
- Samaniego, L. et al. Anthropogenic warming exacerbates European soil moisture droughts. *Nat. Clim. Change* **8**, 421–426 (2018).
- Ciais, P. et al. Europe-wide reduction in primary productivity caused by the heat and drought in 2003. *Nature* **437**, 529–533 (2005).
- Ionita, M. et al. The European 2015 drought from a climatological perspective. *Hydrol. Earth Syst. Sci.* **21**, 1397–1419 (2017).
- Naumann, G., Cammalleri, C., Mentaschi, L. & Feyen, L. Increased economic drought impacts in Europe with anthropogenic warming. *Nat. Clim. Change* **11**, 485–491 (2021).
- Allan, R. P. & Soden, B. J. Atmospheric warming and the amplification of precipitation extremes. *Science* **321**, 1481–1484 (2008).
- Masson-Delmotte, V. et al. *IPCC, 2021: Climate Change 2021: The Physical Science Basis. Contribution of Working Group I to the Sixth Assessment Report of the Intergovernmental Panel on Climate Change* (Cambridge University Press, 2021).
- Chiang, F., Mazdiyasi, O. & AghaKouchak, A. Evidence of anthropogenic impacts on global drought frequency, duration, and intensity. *Nat. Commun.* **12**, 2754 (2021).
- Spinoni, J., Vogt, J. V., Naumann, G., Barbosa, P. & Dosio, A. Will drought events become more frequent and severe in Europe? *Int. J. Climatol.* **38**, 1718–1736 (2018).
- Markonis, Y., Hanel, M., Máca, P., Kysely, J. & Cook, E. R. Persistent multi-scale fluctuations shift European hydroclimate to its millennial boundaries. *Nat. Commun.* **9**, 1767 (2018).
- Marvel, K. et al. Twentieth-century hydroclimate changes consistent with human influence. *Nature* **569**, 59–65 (2019).
- Ionita, M., Dima, M., Nagavciuc, V., Scholz, P. & Lohmann, G. Past megadroughts in central Europe were longer, more severe and less warm than modern droughts. *Commun. Earth Environ.* **2**, 61 (2021).
- Büntgen, U. et al. Recent European drought extremes beyond Common Era background variability. *Nat. Geosci.* **14**, 190–196 (2021).
- Hari, V., Rakovec, O., Markonis, Y., Hanel, M. & Kumar, R. Increased future occurrences of the exceptional 2018–2019 Central European drought under global warming. *Sci. Rep.* **10**, 12207 (2020).
- Cook, E. R. et al. Old World megadroughts and pluvials during the Common Era. *Sci. Adv.* **1**, e1500561 (2015).
- Fritts, H. C. *Tree Rings and Climate* (Academic Press, London and New York, 1976).
- Helle, G. & Schleser, G. Beyond CO₂ fixation by Rubisco—an interpretation of 13C/12C variations in tree rings from novel intra seasonal studies on broad leaf trees. *Plant Cell Environ.* **27**, 367–380 (2004).
- Urban, O. et al. The dendroclimatic value of oak stable isotopes. *Dendrochronologia* **65**, 125804 (2021).
- Boettger, T. T. et al. Wood cellulose preparation methods and mass spectrometric analyses of delta13C, delta18O, and nonexchangeable delta2H values in cellulose, sugar, and starch: an interlaboratory comparison. *Anal. Chem.* **79**, 4603–4612 (2007).
- Treydte, K. et al. Signal strength and climate calibration of a European tree-ring isotope network. *Geophys. Res. Lett.* **34**, 224 (2007).
- Balting, D. F. et al. Large-scale climate signals of a European oxygen isotope network from tree rings. *Clim. Past* **17**, 1005–1023 (2021).
- Linán, I. D. et al. Estimating 750 years of temperature variations and uncertainties in the Pyrenees by tree ring reconstructions and climate simulations. *Clim. Past* **8**, 919–933 (2012).
- Heinrich, I., Touchan, R., Dorado Liñán, I., Vos, H. & Helle, G. Winter-to-spring temperature dynamics in Turkey derived from tree rings since AD 1125. *Clim. Dyn.* **41**, 1685–1701 (2013).
- Haupt, M., Weigl, M., Grabner, M. & Boettger, T. A 400-year reconstruction of July relative air humidity for the Vienna region (eastern Austria) based on carbon and oxygen stable isotope ratios in tree-ring latewood cellulose of oaks (*Quercus petraea* Matt. Liebl.). *Clim. Change* **105**, 243–262 (2010).
- Danis, P. A. et al. Reconstruction of past precipitation Delta18O using tree-ring cellulose Delta18O and Delta13C: a calibration study near Lac d'Annecy, France. *Earth Planet. Sci. Lett.* **243**, 439–448 (2006).
- Rinne, K., Loader, N., Switsur, V. & Waterhouse, J. 400-year May–August precipitation reconstruction for Southern England using oxygen isotopes in tree rings. *Quat. Sci. Rev.* **60**, 13–25 (2013).
- Loader, N. et al. Multiple stable isotopes from oak trees in southwestern Scotland and the potential for stable isotope dendroclimatology in maritime climatic regions. *Chem. Geol.* **252**, 62–71 (2008).
- Weigl, M., Grabner, M., Helle, G., Schleser, G. H. & Wimmer, R. Variability of latewood-widths and stable isotope ratios in a sessile oak tree (*Quercus petraea*). *Dendrochronologia* **24**, 117–122 (2007).
- Andreu Hayles, L. et al. Long tree ring chronologies reveal 20th century increases in water use efficiency but no enhancement of tree growth at five Iberian pine forests. *Glob. Change Biol.* **17**, 2095–2112 (2011).
- Trenberth, K. E. & Shea, D. J. Relationships between precipitation and surface temperature. *Geophys. Res. Lett.* **32**, L14703 (2005).
- Vicente-Serrano, S. & Beguería, S. A multiscalar drought index sensitive to global warming: the standardized precipitation evapotranspiration index. *J. Clim.* **23**, 1696 (2010).
- Babst, F. et al. 500 years of regional forest growth variability and links to climatic extreme events in Europe. *Environ. Res. Lett.* **7**, 045705 (2012).
- Balanzategui, D. et al. An 810-year history of cold season temperature variability for northern Poland. *Boreas* **47**, 443–453 (2018).
- Cook, E. R. et al. Asian monsoon failure and megadrought during the last millennium. *Science* **328**, 486–489 (2010).
- Cook, E. R. Long-term aridity changes in the western United States. *Science* **306**, 1015–1018 (2004).
- Pauling, A., Luterbacher, J., Casty, C. & Wanner, H. Five hundred years of gridded high-resolution precipitation reconstructions over Europe and the connection to large-scale circulation. *Clim. Dyn.* **26**, 387–405 (2005).
- Luterbacher, J., Dietrich, D., Xoplaki, E., Grosjean, M. & Wanner, H. European seasonal and annual temperature variability, trends, and extremes since 1500. *Science* **303**, 1499–1503 (2004).
- Robock, A. Volcanic eruptions and climate. *Rev. Geophys.* **38**, 191–219 (2000).
- Trigo, R. M. et al. Iberia in 1816, the year without a summer. *Int. J. Climatol.* **29**, 99–115 (2009).
- Brönnimann, S. et al. Last phase of the Little Ice Age forced by volcanic eruptions. *Nat. Geosci.* **12**, 650–656 (2019).
- Vaquero, J. & Trigo, R. Revised group sunspot number values for 1640, 1652, and 1741. *Sol. Phys.* **289**, 803–808 (2013).

42. Pompeani, D. P. et al. Severe Little Ice Age drought in the midcontinental United States during the Mississippian abandonment of Cahokia. *Sci. Rep.* **11**, 13829 (2021).
43. Nussbaumer, S. U., Nesje, A. & Zumbühl, H. J. Historical glacier fluctuations of Jostedalbreen and Folgefonna (southern Norway) reassessed by new pictorial and written evidence. *Holocene* **21**, 455–471 (2011).
44. Marcott, S. A., Shakun, J. D., Clark, P. U. & Mix, A. C. A reconstruction of regional and global temperature for the past 11,300 years. *Science* **339**, 1198–1201 (2013).
45. Lewis, S. L. & Maslin, M. A. Defining the Anthropocene. *Nature* **519**, 171–180 (2015).
46. Ludwig, P. et al. Perspectives of regional paleoclimate modeling. *Ann. N. Y. Acad. Sci.* **1436**, 54–69 (2019).
47. Gómez-Navarro, J. J. et al. A regional climate palaeosimulation for Europe in the period 1500–1990 – Part 2: shortcomings and strengths of models and reconstructions. *Clim. Past* **11**, 1077–1095 (2015).
48. Ljungqvist, F. C. et al. Northern Hemisphere hydroclimate variability over the past twelve centuries. *Nature* **532**, 94–98 (2016).
49. Raible, C. C., Bärenbold, O. & Gómez-Navarro, J. J. Drought indices revisited – improving and testing of drought indices in a simulation of the last two millennia for Europe. *Tellus A: Dyn. Meteorol. Oceanogr.* **69**, 1296226 (2017).
50. PAGES Hydro2k Consortium. Comparing proxy and model estimates of hydroclimate variability and change over the Common Era. *Clim. Past* **13**, 1851–1900 (2017).
51. Beguería, S., Vicente-Serrano, S. M. & Martínez, M. A. A multiscalar global drought dataset: the SPEIbase: a new gridded product for the analysis of drought variability and impacts. *Bull. Am. Meteorol. Soc.* **91**, 1351–1354 (2010).
52. Harris, I., Osborn, T. J., Jones, P. & Lister, D. Version 4 of the CRU TS monthly high-resolution gridded multivariate climate dataset. *Sci. Data* **7**, 109 (2020).
53. McCarroll, D. et al. Correction of tree ring stable carbon isotope chronologies for changes in the carbon dioxide content of the atmosphere. *Geochim. Cosmochim. Acta* **73**, 1539–1547 (2009).
54. Suess, H. E. Radiocarbon concentration in modern wood. *Science* **122**, 415–417 (1955).
55. Belmecheri, S. & Lavergne, A. Compiled records of atmospheric CO₂ concentrations and stable carbon isotopes to reconstruct climate and derive plant ecophysiological indices from tree rings. *Dendrochronologia* **63**, 125748 (2020).
56. Schneider, T. Analysis of incomplete climate data: estimation of mean values and covariance matrices and imputation of missing values. *J. Clim.* **14**, 853–871 (2001).
57. Cook, E. R., Meko, D. M., Stahle, D. W. & Cleaveland, M. K. Drought reconstructions for the continental United States. *J. Clim.* **12**, 1145–1162 (1999).
58. Seftigen, K., Cook, E. R., Linderholm, H. W., Fuentes, M. & Björklund, J. The potential of deriving tree-ring based field reconstructions of droughts and pluvials over Fennoscandia. *J. Clim.* **28**, 141231092609003–3471 (2014).
59. Mauget, S. A. Intra-to multidecadal climate variability over the continental United States: 1932–99. *J. Clim.* **16**, 2215–2231 (2003).
60. Fudge, T. J. et al. Onset of deglacial warming in West Antarctica driven by local orbital forcing. *Nature* **500**, 440–444 (2013).
61. Benjamini, Y. & Hochberg, Y. Controlling the false discovery rate: a practical and powerful approach to multiple testing. *J. R. Stat. Soc. Series B* **57**, 289–300 (1995).
62. Babst, F. et al. Site and species specific responses of forest growth to climate across the European continent. *Glob. Ecol. Biogeogr.* **22**, 706–717 (2013).

Acknowledgements

The ISONET project is supported by the European Union (EVK2-CT-2002-00147 'ISONET'). We want to thank all participants of the ISONET project (L. Andreu, Z. Bednarz, F. Berninger, T. Boettger, C. M. D'Alessandro, J. Esper, N. Etien, M. Filot, D. Frank, M. Grabner, M. T. Guillemin, E. Gutierrez, M. Haupt, E. Hilasvuori, H. Jungner, M. Kalela-Brundin, M. Krapiec, M. Leuenberger, H.H. Leuschner, N. J. Loader, V. Masson-Delmotte, A. Pazdur, S. Pawelczyk, M. Pierre, O. Planells, R. Pukiene, C. E. Reynolds-Henne, K. T. Rinne, A. Saracino, M. Saurer, E. Sonninen, M. Stievenard, V. R. Switsur, M. Szczepanek, E. Szychowska-Krapiec, L. Todaro, K. Treydte, J. S. Waterhouse, and M. Weigl). The data from Turkey, Slovenia and Southwest Germany were produced with the EU-funded project MILLENNIUM (GOCE 017008-2 'MILLENNIUM'), special thanks to T. Levanic and R. Touchan. The tree-ring stable isotope chronologies from Bulgaria were established with support of the German Research Foundation DFG (HE3089-1, GR 1432/11-1) and in cooperation with the administration of Pirin National Park, Bulgaria. We also thank E. Cook, D. Benito, E. Zorita, K. Treydte and J. Luterbacher who have inspired, supported and shaped this study.

Author contributions

M.B.F. conceived and designed the study, and led the development of methods, the analysis and the writing of the manuscript with input from G.H., D.F.B., N.B., G.H.S. and U.C. All authors contributed to discussions that shaped the study and the manuscript.

Competing interests

The authors declare no competing interests.

Additional information

Supplementary information The online version contains supplementary material available at <https://doi.org/10.1038/s43247-022-00648-7>.

Correspondence and requests for materials should be addressed to Mandy B. Freund.

Peer review information *Communications Earth & Environment* thanks the anonymous reviewers for their contribution to the peer review of this work. Primary Handling Editors: Joe Aslin and Heike Langenberg.

Reprints and permission information is available at <http://www.nature.com/reprints>

Publisher's note Springer Nature remains neutral with regard to jurisdictional claims in published maps and institutional affiliations.



Open Access This article is licensed under a Creative Commons Attribution 4.0 International License, which permits use, sharing, adaptation, distribution and reproduction in any medium or format, as long as you give appropriate credit to the original author(s) and the source, provide a link to the Creative Commons license, and indicate if changes were made. The images or other third party material in this article are included in the article's Creative Commons license, unless indicated otherwise in a credit line to the material. If material is not included in the article's Creative Commons license and your intended use is not permitted by statutory regulation or exceeds the permitted use, you will need to obtain permission directly from the copyright holder. To view a copy of this license, visit <http://creativecommons.org/licenses/by/4.0/>.

© The Author(s) 2023